Featured in Physics

Experimental Speedup of Quantum Dynamics through Squeezing

S. C. Burd,[1,2,*,§,¶] H. M. Knaack,[1,2,¶] R. Srinivas,[1,2,‖] C. Arenz,[3,†] A. L. Collopy,[1]
L. J. Stephenson,[1,2] A. C. Wilson,[1] D. J. Wineland,[1,2,4] D. Leibfried,[1] J. J. Bollinger,[1]
D. T. C. Allcock,[1,2,4] and D. H. Slichter[1,‡]

[1] *Time and Frequency Division, National Institute of Standards and Technology, 325 Broadway, Boulder, Colorado 80305, USA*
[2] *Department of Physics, University of Colorado, Boulder, Colorado 80309, USA*
[3] *School of Electrical, Computer and Energy Engineering, Arizona State University, Tempe, Arizona 85287, USA*
[4] *Department of Physics, University of Oregon, Eugene, Oregon 97403, USA*

(Received 9 May 2023; revised 4 December 2023; accepted 9 February 2024; published 17 April 2024)

We show experimentally that a broad class of interactions involving quantum harmonic oscillators can be made stronger (amplified) using a unitary squeezing protocol. While our demonstration uses the motional and internal states of a single trapped $^{25}Mg^{+}$ ion, the scheme applies generally to Hamiltonians involving just a single harmonic oscillator as well as Hamiltonians coupling the oscillator to another quantum degree of freedom such as a qubit, covering a large range of systems of interest in quantum information and metrology applications. Importantly, the protocol does not require knowledge of the parameters of the Hamiltonian to be amplified, nor does it require a well-defined phase relationship between the squeezing interaction and the rest of the system dynamics, making it potentially useful in instances where certain aspects of a signal or interaction may be unknown or uncontrolled, such as searches for novel forms of dark matter.

DOI: 10.1103/PRXQuantum.5.020314

I. INTRODUCTION

Quantum mechanical squeezing, where the uncertainty in a desired observable is reduced at the expense of increasing uncertainty in a separate, noncommuting observable, is a powerful technique for quantum-enhanced sensing and measurement [1–8], enabling the detection of extremely weak signals or forces [9–20]. Squeezing can also be used to enhance the strength of interactions between quantum systems, for example by amplifying optomechanical or light-matter interactions relevant in quantum information science [21–33].

The amount of enhancement in sensitivity or interaction strength that can be achieved depends not just on the strength and fidelity of the squeezing operations, but also on their timing and phase relationship relative to the other parameters in the system Hamiltonian, including the signal to be sensed or the interaction to be enhanced. In some applications, the required phases and timings for squeezing operations relative to the rest of the system dynamics may be sufficiently stable that they can be calibrated in advance. However, in other instances the parameters of the Hamiltonian may be unknown or fluctuate in time, such that naïve application of squeezing operations can give rise to undesired "error" dynamics in the system in addition to the desired enhancement.

The recently proposed scheme of "Hamiltonian amplification" (HA) provides a method to achieve squeezing-based enhancement of dynamics involving a quantum harmonic oscillator where parameters are fluctuating or unknown [27,34]. By stroboscopically applying squeezing transformations with alternating phases, errors due to unknown phase relationships are dynamically suppressed, while the desired interactions are strengthened (amplified). Crucially, the protocol does not require knowledge of the parameters of the Hamiltonian to be amplified as long as it can be written in a certain form and the timescales for the bare Hamiltonian dynamics are slow compared to the duration of applied squeezing operations.

*scburd@stanford.edu
†carenz1@asu.edu
‡daniel.slichter@nist.gov
§Current address: Department of Physics, Stanford University, Palo Alto, California, USA.
‖Current address: Department of Physics, University of Oxford, Oxford, UK.
¶These authors contributed equally to this work.

In this work, we experimentally realize Hamiltonian amplification using the motion of a trapped atomic ion as the quantum harmonic oscillator. As proof of principle, we use HA to demonstrate phase-insensitive amplification of coherent displacements of the ion motion, with a gain of approximately 2 as the relative phase of the displacement is swept across the full range of 2π. We also perform phase-insensitive enhancement of laser-induced coupling between the trapped ion's motion and its internal electronic "spin" state, where the phase of the laser interaction is not stable with respect to that of the squeezing interaction, observing an increase in the effective spin-motion coupling strength of approximately 1.5.

II. THEORETICAL BACKGROUND

The coupling of a particular quantum harmonic oscillator with Hamiltonian $\hat{H} = \hbar\omega\hat{a}^\dagger\hat{a}$ to another quantum system or to an external resonant driving field (that results in a signal to be sensed) can be described in the interaction picture with respect to the bare oscillator Hamiltonian (and all terms not involving the chosen harmonic oscillator) by a Hamiltonian of the form

$$\hat{H} = \hbar\Omega(\hat{\beta}\hat{a}^\dagger + \hat{\beta}^\dagger\hat{a}). \tag{1}$$

Here, $\hat{a}$ and $\hat{a}^\dagger$ are the annihilation and creation operators of the chosen harmonic oscillator, ω is the harmonic oscillator frequency, and Ω characterizes the interaction strength with either an external driving field—in which case $\hat{\beta}$ is just a complex number—or a second quantum system, where $\hat{\beta}$ is an operator for that system. For example, in the case where $\hat{\beta} = \hat{\sigma}^-$, the lowering operator for a two-level system represented by a spin-1/2 particle, Eq. (1) is a Jaynes-Cummings-type coupling. However, in general, the operator $\hat{\beta}$ describing the second quantum system does not need to be specified for the HA procedure to work, which makes the method amenable to amplifying interactions in a wide range of systems. This is true even when $\hat{\beta}$ is unknown, for example in the case of sensing dark matter that couples to the harmonic oscillator.

An external resonant driving field with constant amplitude applied to the harmonic oscillator for a duration t_d will cause a coherent displacement from the time evolution $\exp(-i\hat{H}t_d/\hbar) = \hat{D}(\alpha)$, where $\hat{D}(\alpha) \equiv \exp(\alpha\hat{a}^\dagger - \alpha^*\hat{a})$ is the displacement operator and $\alpha = -i\Omega\beta t_d$, where we have dropped the hat from β since here it is just a complex number and not an operator. Measuring the displacement α constitutes sensing of the external field during t_d. If $|\alpha| \ll 1$ (sensing a very weak signal), amplifying the displacement will enable it to be more easily resolved with respect to the zero-point fluctuations of the harmonic oscillator, which set the noise floor for measuring displacements. The desired amplification can be achieved by applying appropriate squeezing and antisqueezing operations before and after the sensing period according to the identity [11,35]

$$\hat{S}^\dagger(\xi)\hat{D}(\alpha)\hat{S}(\xi) = \hat{D}(\alpha_{\text{amp}}). \tag{2}$$

Here $\hat{S}(\xi) = \exp((\xi^*\hat{a}^2 - \xi\hat{a}^{\dagger 2})/2)$ is the squeezing operator with the complex squeezing parameter $\xi = r\exp(i\theta)$, and the amplified displacement is given by $\alpha_{\text{amp}} = \alpha\cosh(r) + \alpha^* e^{i\theta}\sinh(r)$, where r is taken to be real and positive. The angle θ describes the quadrature of the harmonic oscillator that is squeezed by the application of $\hat{S}(\xi)$. In harmonic oscillator phase space, viewed in the frame rotating at ω, the squeezed axis makes an angle of $\theta/2$ with respect to the real axis.

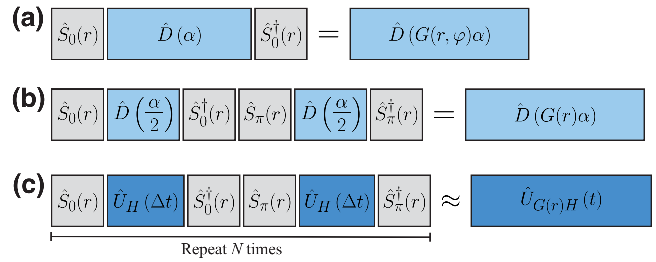

FIG. 1. Pulse sequences for different quantum amplification schemes using unitary squeezing. (a) Pulse sequence for the phase-sensitive amplification scheme used in Ref. [11]. (b) Pulse sequence for Hamiltonian amplification of a coherent displacement. (c) Pulse sequence for Hamiltonian amplification of a general interaction as in Eq. (5), which must be appropriately Trotterized [36,37].

The pulse sequence corresponding to Eq. (2) is shown in Fig. 1(a). Both the magnitude and the phase of the amplitude gain $G \equiv \alpha_{\text{amp}}/\alpha$ depend on the phase relationship between the displacement and the squeezing, with $G(r,\varphi) = \cosh(r) + e^{i(\theta-2\varphi)}\sinh(r)$, where $\varphi = \arg(\alpha)$ is the phase of the displacement in the previously described rotating frame of the harmonic oscillator. Achieving maximum gain requires that $\theta - 2\varphi = 2n\pi$ for integer n, giving $G = e^r$; fluctuations in this phase difference will cause corresponding gain fluctuations, and for some values of the phase, the displacement will even be deamplified, with $|G| < 1$. Depending on the nature of the physical system, it may be challenging to stabilize θ and φ with respect to each other.

Therefore, we seek to perform phase-independent amplification, where G is independent of θ and φ. For amplification of displacements, this can be achieved by dividing the displacement into two steps, $\hat{D}(\alpha) = \hat{D}(\alpha/2)\hat{D}(\alpha/2)$, and amplifying each step individually with squeezing and antisqueezing operations. Crucially, the second step is amplified along the harmonic oscillator quadrature that is 90° out of phase with respect to the quadrature along which the first step is amplified; mathematically, the value of θ is increased by π for the second squeeze-antisqueeze pair. Without loss of generality, we

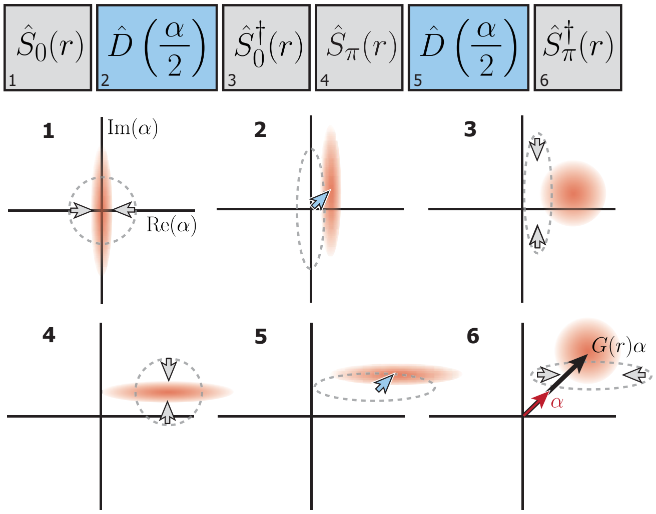

FIG. 2. Schematic of Hamiltonian amplification of a coherent displacement. We plot a series of schematic representations of the motional phase space distribution, before (dotted gray outline) and after (orange) each numbered pulse. The arrows indicate squeezing (gray) and displacement (blue) operations, respectively. In the final panel, the red arrow shows the total unamplified displacement, while the black arrow shows the amplified displacement, which points in the same direction, but is larger by a factor $G(r)$.

can take the values of θ to be 0 and π for the first and second squeeze-antisqueeze pairs, respectively. The sequence of operations, shown in Fig. 1(b) and also in Fig. 2, is now

$$\hat{D}(\alpha_{\text{amp}}) = \hat{S}_\pi^\dagger(r)\hat{D}(\alpha/2)\hat{S}_\pi(r)\hat{S}_0^\dagger(r)\hat{D}(\alpha/2)\hat{S}_0(r), \tag{3}$$

where the subscripts on $\hat{S}$ indicate the value of θ. We note the identity $\hat{S}_0^\dagger(r) = \hat{S}_\pi(r)$, such that the second pair of squeezing pulses are identical to the first pair but with reversed order. Using the identity in Eq. (2), and the fact that the product of two displacement operators is just another displacement operator times a complex phase, we find that $\hat{D}(\alpha_{\text{amp}}) = \exp(\cosh(r)(\alpha\hat{a}^\dagger - \alpha^*\hat{a}))$, up to a global phase. As such, the sequence in Eq. (3) yields a gain of

$$G(r) = \cosh(r), \tag{4}$$

independent of the phases θ and φ. The price for phase insensitivity is a reduction in the gain G relative to the maximum achievable with the phase-sensitive scheme in Eq. (2); for $r \gtrsim 1$, the gain is reduced by a factor of approximately 2.

The situation is somewhat more complicated when squeezing is used to amplify general interactions of the form of Eq. (1), where $\hat{\beta}$ is an operator and not a complex number. Consider a time evolution modified through instantaneous squeezing and antisqueezing, performed sequentially along two orthogonal quadratures in phase space according to

$$\hat{U}(t) = \hat{S}_\pi^\dagger(r)\hat{U}_H(t/2)\hat{S}_\pi(r)\hat{S}_0^\dagger(r)\hat{U}_H(t/2)\hat{S}_0(r), \tag{5}$$

where $\hat{U}_H(t) = \exp(-i\hat{H}t/\hbar)$ describes the time evolution for a time interval t under the Hamiltonian in Eq. (1). In general, Eq. (5) yields an infinite power series in t, giving "error" terms in addition to the desired amplified interaction. To address this, we can Trotterize the interaction [36,37], splitting the total interaction time t into small segments $\Delta t = t/2N$ with integer N such that $\hat{U}(t) = [\hat{U}(2\Delta t)]^N$ and repeating the sequence in Eq. (5) N times. For sufficiently large N (or, equivalently, sufficiently small Δt), we can neglect higher-order terms in Δt and find that

$$\hat{U}_{G(r)H}(t) \approx \exp(-i\cosh(r)\hat{H}t/\hbar). \tag{6}$$

In this regime, the system dynamics are approximately governed by an amplified Hamiltonian $\hat{H}_{\text{amp}} = G(r)\hat{H}$ with phase-independent gain $G(r) = \cosh(r)$, thus the name "Hamiltonian amplification" [27]. We remark here that while the sequence given in Eq. (5) rests on the assumption that the evolution generated by the interaction $\hat{H}$ can be neglected during squeezing, this assumption is in general not necessary for HA to work. Large, smooth, high-frequency modulations of the squeezing parameter can be used instead to achieve amplification of interactions in systems where this assumption cannot be met. We refer the reader to Ref. [27] and Appendix B for further details. Developing a valid description of the open quantum harmonic oscillator system driven by infinitely strong and fast parametric controls is challenging and will be the subject of future studies. According to the Trotter formula, the dynamics in Eq. (6) become exact in the limit of $N \to \infty$ [27,34]. For finite N, it is generally challenging to bound the Trotter error for systems with infinite-dimensional Hilbert spaces [38]. However, a rough estimate for the required fineness of the Trotterization is given by the scaling of the second-order term in Δt, yielding $\Delta t \ll [\Omega\sqrt{\sinh(2r)}]^{-1}$, ignoring the dependence of the estimate on the operators in this second order term [27]. This corresponds to a number of required Trotter steps $N \gg \Omega t\sqrt{\sinh(2r)}/(2\cosh(r))$ for a total unamplified interaction duration t; in the limit $r \to 0$ no Trotterization is required, while, for $r \gtrsim 1$, we find that $N \gg \Omega t/\sqrt{2}$ (see Appendix C).

III. EXPERIMENTAL SETUP

The experiment uses a single $^{25}Mg^+$ ion confined in a surface-electrode ion trap [39] containing current-carrying electrodes for producing strong near-field magnetic field gradients at the ion position, 30 μm above the electrode plane. Details of the experimental apparatus have been presented elsewhere [11,40–42]. The harmonic oscillator degree of freedom is a radial mode of ion motion with frequency $\omega/2\pi \sim 7$ MHz, whose state we describe in the number state basis $|n\rangle$. This motional mode is the same one used in Ref. [11], with a heating rate of 20(3) quanta per second and a motional dephasing rate of 18(6) s^{-1}. The ion motion is cooled near its ground state (mean phonon occupation $\bar{n} = 0.06$) by Doppler cooling with laser light at 280 nm followed by resolved sideband cooling [43]. Preparation and analysis of the motional quantum state rely on coupling the motion to a qubit encoded in the internal (electronic) states of the ion via motional sideband transitions [44,45]. We choose the $|\downarrow\rangle \equiv |F = 3, m_F = 1\rangle$ and $|\uparrow\rangle \equiv |F = 2, m_F = 1\rangle$ states of the $^2S_{1/2}$ electronic ground-state hyperfine manifold as qubit states (qubit frequency $\omega_q/2\pi = 1.686$ GHz with a quantization magnetic field of 21.3 mT), and implement sideband transitions for cooling and motional state analysis using near-field magnetic field gradients oscillating at $\omega_q \pm \omega$ [46,47]. Coherent displacements of the motional state are performed by applying a resonant electric potential at ω to a trap electrode—producing a corresponding oscillating and approximately spatially uniform electric field at the ion—for a fixed duration [11,44]. Squeezing and antisqueezing of the motional state is achieved by applying an electric potential to the trap rf electrodes at frequency 2ω, which parametrically modulates the confining potential [11,41,48]. The magnitude r of the squeezing parameter can be adjusted either by varying the squeezing pulse duration t_s or by changing the amplitude of the parametric drive and thus the parametric modulation strength g, since $r = gt_s$ (see Appendix D). The electronic waveforms used to implement the resonant and parametric drives are generated using phase-synchronized direct digital synthesizers. By adjusting the relative phase of these waveforms, we can arbitrarily control the squeezing angle θ and the displacement direction φ in motional phase space. For all sequences, we characterize the initial and final motional states using a magnetic gradient-based blue sideband (BSB) analysis pulse that couples the motional state to the internal qubit states of the ion. By measuring the qubit state populations for varying BSB pulse durations, we can extract the motional Fock state populations (the diagonal elements of the motional state density matrix in the Fock basis; see Appendix D) [49]. We then characterize the measured states by fitting the extracted Fock state populations to parameterized models of Fock state populations corresponding to either coherent states or displaced squeezed states (see Fig. 6 below and Appendix D). We verify the phase coherence of squeezed states by antisqueezing them and verifying that the motion returns to near the ground state (see Appendix D) [11].

IV. RESULTS

We first perform HA of coherent displacements, a method that could be used for quantum-enhanced sensing of unknown weak resonant fields, using the pulse sequence in Fig. 1(b). The squeezing and displacement operations have durations of $t_s = 2.75$ μs and $t_d = 7$ μs, respectively. To characterize the phase sensitivity of the protocol, we perform the same amplification sequence with fixed θ for ten different values of φ uniformly spaced to cover the interval $[0, 2\pi)$, and measure the resulting gain. We calibrate the displacement strength by setting $r = 0$ (replacing squeezing with a delay of equivalent duration), measuring a coherent state amplitude $\alpha_i = 0.55(2)$. The squeezing strength $r = 1.38(8)$ is extracted by squeezing the initial state (approximately the ground state) and fitting the resulting Fock state populations (see Appendix D). With the squeezing turned on in the HA sequence, we measure a mean final displacement amplitude (averaged over all displacement phases) of $\alpha_{\rm amp} = 0.979(3)$; data are shown in Fig. 3. The corresponding mean gain is $G = 1.77(5)$, in reasonable agreement with the theoretically expected gain of $\cosh(r) = 2.11(15)$. We see some residual phase dependence of the gain due to imperfect calibration of the strengths and phases of the squeezing pulses, as well as drifts in the squeeze drive (see Appendix D). We can also perform this HA by subdividing α_i more finely and performing a generalized HA sequence with N rounds, as shown in Fig. 1(c). No Trotterization error occurs when amplifying a coherent displacement, so we can choose any value of N. We find that increasing N improves the phase insensitivity at the cost of decreased overall gain (see Fig. 7 below), which we believe is due to amplified motional

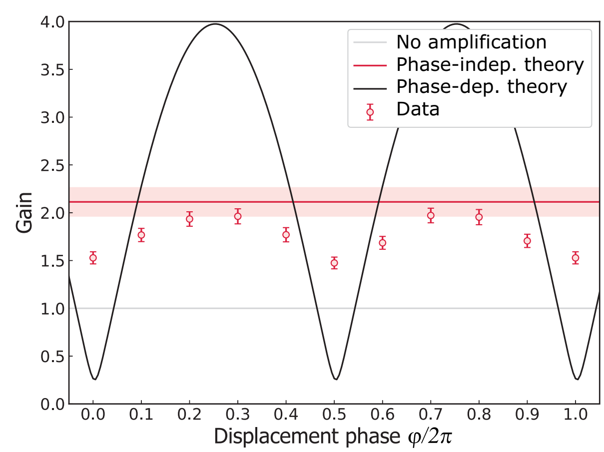

FIG. 3. HA gain versus displacement phase. Experimental data are shown as red circles, with error bars denoting 68% confidence intervals. The red line (light red band) shows the theoretical prediction (68% confidence interval) for the HA gain $G = \cosh(r)$ given the experimentally determined value of $r = 1.38(8)$. The theoretical phase-dependent gain of the scheme in Fig. 1(a) given the same r is shown for comparison as the black line. The gray line denotes $G = 1$. The data point plotted at $\varphi/2\pi = 1$ is a copy of the data point at $\varphi/2\pi = 0$.

decoherence from the additional squeezing pulses, as well as imperfect pulse calibrations.

Next, we demonstrate the use of HA to enhance the coupling between a quantum harmonic oscillator and a qubit, characterized by state transition operators $\hat{\sigma}^{\pm} \equiv \frac{1}{2}(\hat{\sigma}_x \mp i\hat{\sigma}_y)$ constructed from Pauli operators $\hat{\sigma}_x$ and $\hat{\sigma}_y$. In our experiment, we can drive a red sideband (RSB) transition on the ion to realize the Jaynes-Cummings (JC) Hamiltonian

$$\hat{H}_{\rm JC} = \hbar\Omega(\hat{\sigma}^- \hat{a}^\dagger + \hat{\sigma}^+ \hat{a}), \tag{7}$$

where the qubit states $|\tilde{\downarrow}\rangle \equiv {}^2S_{1/2}\,|F=3, m_F=3\rangle$ and $|\tilde{\uparrow}\rangle \equiv {}^2S_{1/2}\,|F=2, m_F=2\rangle$ have energy splitting $\hbar\widetilde{\omega}_q$, with $\widetilde{\omega}_q/2\pi = 1.326$ GHz, and the harmonic oscillator is a motional mode of the ion. The qubit-harmonic oscillator coupling is realized with a laser-driven stimulated Raman transition [44], using two noncopropagating laser beams at 280 nm with a frequency difference of $\widetilde{\omega}_q - \omega$. We choose a different pair of hyperfine states ($|\tilde{\uparrow}\rangle$ and $|\tilde{\downarrow}\rangle$) as the qubit due to experimental constraints on the frequency difference of the Raman laser beams. The phase of the RSB interaction is determined by the (unstabilized) phase of the optical beat note of the two laser beams at the ion, which is sensitive to differential optical path length fluctuations for the two beams and can vary over a substantial fraction of 2π between successive experimental trials. Amplifying these dynamics with HA again demonstrates that HA is phase independent, since otherwise individual experimental shots would exhibit widely varying gain, including gains below 1 (deamplification) [41].

Amplification of $\hat{H}_{\rm JC}$ is achieved by interleaving a sequence of laser-induced red sideband pulses with squeezing pulses, as shown in Fig. 1(c). Since $[\hat{H}_{\rm JC}, \hat{S}(\xi)]$ is an operator and not a complex number, a Trotterized HA sequence with sufficiently high N is required for faithful amplification of the Hamiltonian according to Eq. (6); experimentally, we find that $N = 6$ strikes a balance between giving qualitatively small "error" terms from Trotterization and minimizing motional decoherence arising from imperfect squeezing pulses. These experiments used longer, weaker squeezing pulses ($t_s = 6$ μs with smaller g) to help reduce the residual effects of imperfections in the squeezing, at the cost of increased squeezing duration. The JC interaction induces Rabi oscillations between the $|\tilde{\uparrow}\rangle\,|n=0\rangle$ and $|\tilde{\downarrow}\rangle\,|n=1\rangle$ states with Rabi frequency Ω. Figure 4 shows the population in the $|\tilde{\uparrow}\rangle$ state as a function of the total duration of the Trotterized laser sideband pulses applied (the duration of the squeezing pulses, which is 144 μs total for $N = 6$, is not included). We measure an increase in Ω by a factor of 1.56(2) (determined by fitting to an exponentially decaying sinusoid) under HA with a squeezing parameter $r = 1.1(1)$, relative to the case without squeezing ($r = 0$), as shown in Fig. 4. For comparison, the theoretically expected gain from HA is $\cosh r = 1.7(1)$.

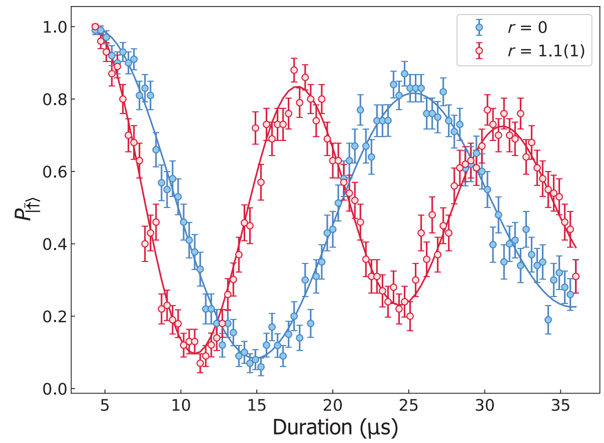

FIG. 4. Hamiltonian amplification of the Jaynes-Cummings (JC) interaction. Population in $|\tilde{\uparrow}\rangle$ as a function of the JC interaction duration for a Hamiltonian amplification sequence with $N = 6$. For the amplified case (red data points and fit line), the duration of the squeezing pulses is not included (see the main text). The JC interaction induces Rabi oscillations between the $|\tilde{\uparrow}\rangle\,|n=0\rangle$ and $|\tilde{\downarrow}\rangle\,|n=1\rangle$ states with a rate Ω. Increasing the squeezing parameter from $r = 0$ to $r = 1.1$ increases Ω by a factor of 1.56(2). The solid lines are fits to exponentially decaying sinusoids. Error bars indicate 68% confidence intervals.

Because the JC interaction being amplified in this proof-of-principle demonstration is already relatively strong compared to the parametric driving (in the sense that $\Omega \approx g$), the use of HA does not provide a speedup when one considers the total duration including that of the squeezing pulses (a "wall clock" speedup). For sensing tasks, the interaction may be very weak ($\Omega \ll g$), in which case HA can provide a substantial wall clock speedup. In general, for Trotterized Hamiltonians, wall clock speedup can be achieved when $g \gtrsim 20\Omega$, while when Trotterization is not needed, wall clock speedup is achieved for $gt \gtrsim 6$ (see Appendix C). We could increase g in future experiments by using shaped pulse envelopes for the parametric modulation; this reduces ringing and resultant experimental imperfections in squeezing, enabling stronger parametric driving.

We theoretically calculate that HA speeds up dephasing of the motional degrees of freedom as well as the interaction (see Appendix A). However, decoherence processes that occur solely in the coupled system represented by $\hat{\beta}$ are unaffected by HA, making this technique potentially valuable in practice for systems where such decoherence presents a limit. For example, in the instance of the laser-driven JC interaction, qubit decoherence due to off-resonant scattering of Raman laser beams can be reduced because the interaction duration—and thus total scattering error—is smaller under HA, similar to Ref. [41].

In summary, we have implemented the proposed method of Hamiltonian amplification of Ref. [27] in a trapped-ion system. The method can be used in any physical system where fast unitary squeezing can be implemented. For example, low-noise, phase-insensitive amplification of coherent displacements of the electromagnetic field in a cavity could improve the sensitivity of axion dark matter detectors [10,17,50]. In quantum information and simulation platforms where boson-mediated interactions are essential for generating entanglement, Hamiltonian amplification could potentially mitigate the impact of qubit decoherence [41], without requiring phase stabilization between the applied squeezing and the boson-mediated interactions.

ACKNOWLEDGMENTS

We thank A. L. Carter and A. D. Brandt for helpful comments on the manuscript. This work was supported by NIST (https://ror.org/05xpvk416).

C.A. conceived of the HA scheme and developed the theory; S.C.B. and H.M.K. performed the experiments and analyzed the data, assisted by R.S., A.L.C., L.J.S., and D.H.S.; the manuscript was written by D.H.S., C.A., S.C.B., and H.M.K., with input from all authors; D.H.S. and D.T.C.A. supervised the work with support from D.L., A.C.W., J.J.B., and D.J.W.; A.C.W., D.L., D.J.W., and D.H.S. secured funding for the work; all authors contributed to scientific discussions and planning.

APPENDIX A: HAMILTONIAN AMPLIFICATION IN THE PRESENCE OF BOSONIC DEPHASING

We consider a composite system described by the Hamiltonian $\hat{H} = \hbar\Omega(\hat{\beta}\hat{a}^\dagger + \hat{\beta}^\dagger\hat{a})$. We assume that the quantum harmonic oscillator represented by annihilation and creation operators $\hat{a}$ and $\hat{a}^\dagger$ is subject to dephasing described by the dissipator [51]

$$\mathcal{D}_a(\cdot) = -\Gamma[\hat{a}^\dagger\hat{a}, [\hat{a}^\dagger\hat{a}, (\cdot)]], \tag{A1}$$

where nonunitary processes of the system ($\hat{\beta}$) interacting with the quantum harmonic oscillator are described by a dissipator $\mathcal{D}_\beta$, which we do not specify further. Here $(\cdot)$ is a placeholder for the density operator [52]. The total system (i.e., coherent and dissipative parts) is described by a Lindbladian of the form

$$\mathcal{L}(\cdot) = -\frac{i}{\hbar}[\hat{H}, (\cdot)] + \mathcal{D}_a(\cdot) + \mathcal{D}_\beta(\cdot). \tag{A2}$$

The system dynamics at time t is then given by the completely positive and trace-preserving map $\Lambda_t = \exp(\mathcal{L}t)$. Now, we modify the dynamics by alternating in time intervals $\Delta t = t/2N$ between instantaneously squeezing in two quadratures of the harmonic oscillator, described by the unitary maps $\mathcal{S}_0(\cdot) = \hat{S}_0^\dagger(\cdot)\hat{S}_0$ and $\mathcal{S}_\pi(\cdot) = \hat{S}_\pi^\dagger(\cdot)\hat{S}_\pi$, respectively, to realize the Hamiltonian amplification protocol. In the limit of infinitely fast alternation between squeezing quadratures, the dynamics are given by

$$\lim_{N\to\infty}(\mathcal{S}_\pi^\dagger\Lambda_{\Delta t}\mathcal{S}_\pi\mathcal{S}_0^\dagger\Lambda_{\Delta t}\mathcal{S}_0)^N = e^{\bar{\mathcal{L}}t}, \tag{A3}$$

where the effective Lindbladian $\bar{\mathcal{L}}$ reads [53]

$$\bar{\mathcal{L}}(\cdot) = \frac{1}{2}\sum_{j\in\{0,\pi\}}(-i[\mathcal{S}_j(H), (\cdot)] + \mathcal{S}_j^\dagger\mathcal{D}_a(\mathcal{S}_j(\cdot))) + \mathcal{D}_\beta(\cdot). \tag{A4}$$

After some algebra, and using standard properties of the squeezing operator, we find that

$$\begin{aligned}\bar{\mathcal{L}}(\cdot) = &-i\cosh(r)[\hat{H}, (\cdot)] + \cosh^2(2r)\mathcal{D}_a(\cdot)\\ &+ \frac{1}{4}\sinh^2(2r)[\hat{a}^{\dagger 2} + \hat{a}^2, [\hat{a}^{\dagger 2} + \hat{a}^2, (\cdot)]]\\ &+ \mathcal{D}_\beta(\cdot).\end{aligned} \tag{A5}$$

Thus, while the coherent part is amplified by a factor $\lambda = \cosh(r)$, the dephasing $\mathcal{D}_a$ of the quantum harmonic oscillator is amplified by a larger factor $\cosh^2(2r)$. Moreover, we see that $\mathcal{D}_a$ is not just amplified, but also modified under HA, with an additional dephasing-type term appearing in the second line of Eq. (A5) for the effective Lindbladian. We note that the nonunitary process generated by $\mathcal{D}_\beta$, which acts on the system described by $\hat{\beta}$ and $\hat{\beta}^\dagger$ that interacts with the quantum harmonic oscillator, is not amplified or modified by HA. For example, if $\hat{\beta} = \hat{\sigma}^-$ such that $\hat{H}$ is the Jaynes-Cummings interaction then $\mathcal{D}_\beta(\cdot)$ describes decoherence of the qubit coupled to the harmonic oscillator. If this decoherence is dominated by spontaneous off-resonant photon scattering due to the Raman beams generating the Jaynes-Cummings interaction, then the HA process may increase the desired interaction strength without increasing the decoherence rate, thus improving the fidelity of the interactions. However, future work is needed to assess the validity of describing the open system dynamics in the presence of HA (i.e., an open system subject to infinitely strong and fast applied periodic parametric controls) through a Lindblad-type master equation of the form (A2). In fact, in a similar setting it has been argued that such a description of the open system dynamics can fail [53].

APPENDIX B: HAMILTONIAN AMPLIFICATION WITH SMOOTH PULSES

The theoretical derivation of HA in Ref. [27] uses the rapid application of delta-function-like parametric pulses that instantaneously produce the squeezing transformations $\hat{S}_0$ and $\hat{S}_\pi$. In this formulation of HA it is assumed that during the parametric pulse the free evolution governed by the interaction $\hat{H}$ in Eq. (1) can be neglected. However, as we show in more detail below, following the framework described in Ref. [27] and the theory of continuous dynamical decoupling in general [54], this assumption is not needed for HA to work.

We consider a time-dependent Hamiltonian of the form

$$\hat{H}_{\mathrm{tot}}(t) = \hat{H} + \hat{H}_c(t), \tag{B1}$$

where $\hat{H}$ describes the interaction we want to amplify and $\hat{H}_c(t) = i\hbar g(t)(\hat{a}^2 - \hat{a}^{\dagger 2})/2$ describes the parametric drive. If we assume that the modulation $g(t)$ of the parametric drive strength is periodic with a period given by T_c, at times $T = NT_c$ the dynamics is governed by the unitary transformation

$$\hat{U}(NT_c) = \exp(-iT\hat{\bar{H}}), \tag{B2}$$

where $\hat{\bar{H}}$ is given by the Magnus expansion. The first order $\hat{\bar{H}}^{(0)}$ of the Magnus expansion is

$$\hat{\bar{H}}^{(0)} = \frac{1}{T_c}\int_0^{T_c} \hat{U}_c^{\dagger}(t)\hat{H}\hat{U}_c(t)dt, \tag{B3}$$

where $\hat{U}_c(t) = \exp(R(t)(\hat{a}^{\dagger 2} - \hat{a}^2))$ is the evolution generated by the parametric drive alone and $R(t) = \frac{1}{2}\int_0^t g(t')dt'$ is the integrated parametric modulation strength. For sufficiently small T_c, the higher orders of the Magnus expansion can be neglected, so that the dynamics are approximately governed by $\hat{\bar{H}}^{(0)}$ [54]. In this setting HA is achieved when $\hat{\bar{H}}^{(0)}$ becomes $\hat{\bar{H}}^{(0)} = G\hat{H}$, where the amplification factor G depends on the amplitude of the parametric pulse $g(t)$. It can be shown [27] that the pulse

$$g(t) = \frac{2\pi A}{T_c}\cos\left(\frac{2\pi t}{T_c}\right) \tag{B4}$$

achieves $G = I_0(A)$, where $I_0(A)$ is the modified Bessel function of the first kind. As such, a smooth pulse of high frequency $\propto 1/T_c$ and high amplitude $\propto A/T_c$ suppresses the higher order of the Magnus expansion. Thus, the pulse given in Eq. (B4) can achieve HA when the interaction $\hat{H}$ cannot be turned on and off at will.

APPENDIX C: WALL CLOCK SPEEDUP WITH HAMILTONIAN AMPLIFICATION

While HA can be used to strengthen an interaction, and thus reduce the time required to perform a certain amount of desired Hamiltonian evolution, in practice this requires the use of squeezing pulses with finite duration. For a pulsed squeezing scheme as described in the main text (as opposed to continuous smoothly modulated parametric driving as in Appendix B), we consider whether HA can produce a "wall clock" speedup, where the total duration under HA (the sum of the amplified evolution duration and the duration of all the squeezing pulses used in the HA protocol) is less than the duration of the simple unamplified evolution. The question is whether the strengthening of the interactions through HA is outweighed by the time required to perform the necessary squeezing.

We consider the case of a total evolution duration T_0 of the unamplified Hamiltonian in Eq. (1). In the non-Trotterized case, the total evolution duration under HA is given by

$$T_{\mathrm{HA}} = \frac{T_0}{\cosh(r)} + 4t_s, \tag{C1}$$

where the first term is the duration of the amplified evolution and the second is the duration of the squeezing pulses. We can write t_s in terms of r and g, giving

$$T_{\mathrm{HA}} = T_0\left(\frac{1}{\cosh(r)} + \frac{4r}{gT_0}\right). \tag{C2}$$

If the quantity in parentheses is less than 1, HA achieves a wall clock speedup. In Fig. 5(a), we plot T_{HA}/T_0 versus the dimensionless product gT_0 for several values of r. We find a wall clock speedup ($T_{\mathrm{HA}}/T_0 < 1$) in general when $gT_0 \gtrsim 6$ provided $r \gtrsim 1$. Thus, to achieve a wall clock

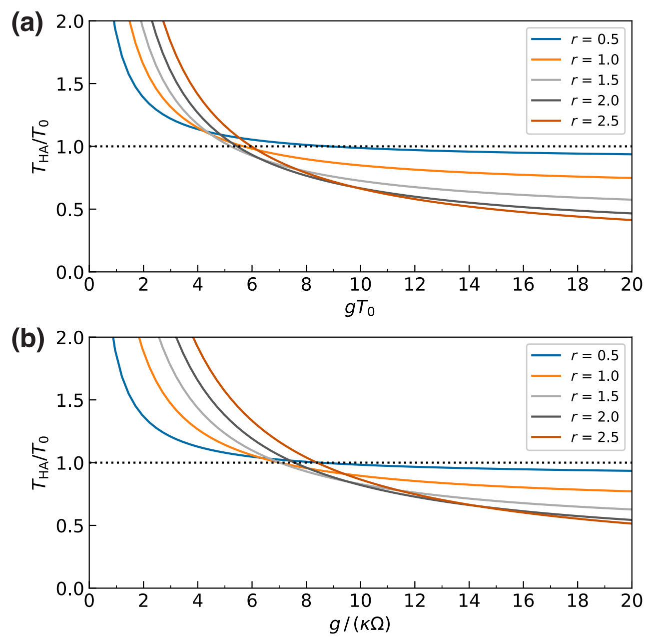

FIG. 5. Wall clock speedup. We plot the ratio of total durations with and without HA, T_{HA}/T_0, for a range of values of r. The two panels show the cases without (a) and with (b) Trotterization during HA. The black dotted lines indicate the wall clock speedup threshold $T_{\mathrm{HA}}/T_0 = 1$.

speedup with HA when sensing small coherent displacements of the harmonic oscillator, the duration T_0 of the sensing probe must be substantially longer than the inverse of the parametric drive strength g.

For Hamiltonian amplification where Trotterization is required, we must account for the dependence of the number of required Trotter steps on the squeezing parameter r as well as the total unamplified duration T_0. The duration of the amplified interaction is equal to the sum of all the Trotterized durations,

$$\frac{T_0}{\cosh(r)} = 2N\Delta t, \tag{C3}$$

which can be combined with the expression for the required Trotterization fineness $\Delta t \ll [\Omega\sqrt{\sinh(2r)}]^{-1}$ and solved for N to yield

$$N \gg \frac{\Omega T_0}{2}\frac{\sqrt{\sinh(2r)}}{\cosh(r)}, \tag{C4}$$

which becomes $N \gg \Omega T_0/\sqrt{2}$ in the limit $r \gtrsim 1$. Physically, this means that every "swap" between the harmonic oscillator and the system described by $\hat{\beta}$ needs to be split into a few Trotter steps.

The total duration under HA (interaction duration plus squeezing duration) given $2N$ Trotter steps is

$$T_{\mathrm{HA}} = \frac{T_0}{\cosh(r)} + 4Nt_s. \tag{C5}$$

We can turn Eq. (C4) into an equality as

$$N = \frac{\kappa\Omega T_0}{2}\frac{\sqrt{\sinh(2r)}}{\cosh(r)}, \tag{C6}$$

where $\kappa \gg 1$ is a dimensionless constant that describes the fineness of the Trotterization. Substituting Eq. (C6) into Eq. (C5), and using $t_s = r/g$, yields

$$T_{\mathrm{HA}} = T_0\left(\frac{1}{\cosh(r)} + \frac{2\kappa r\Omega\sqrt{\sinh(2r)}}{g\cosh(r)}\right). \tag{C7}$$

We plot T_{HA}/T_0 versus the dimensionless quantity $g/(\kappa\Omega)$ in Fig. 5(b) for several values of r, seeing that wall clock speedup occurs when $g/(\kappa\Omega) \gtrsim 7$ (depending on r). Taking a rough guide of $\kappa \gtrsim 3$, we can state that wall clock speedup would require $g \gtrsim 20\Omega$. In other words, the strength of the parametric driving must be considerably greater than the strength of the interaction being amplified in order for HA with Trotterization to produce a net speedup when accounting for the duration of squeezing pulses.

APPENDIX D: MOTIONAL STATE ANALYSIS

Analysis of the motional state populations is accomplished by preparing the desired motional state with the qubit in the $|\downarrow\rangle$ state, then applying a magnetic gradient-based BSB interaction to couple the motional state to the qubit states. This maps information about the motional state onto the qubit state; by measuring the population in the qubit $|\downarrow\rangle$ state using fluorescence detection for varying durations of the BSB interaction, we can extract the state populations in the motional Fock basis. For an arbitrary motional state, the measured population in $|\downarrow\rangle$ is given by [11,49,55]

$$P_\downarrow(t) = \frac{1}{2}\left[1 + \sum_{n=0}^{\infty} P_n e^{-\gamma\sqrt{n+1}t}\cos(\Omega_{\mathrm{SB}}\sqrt{n+1}t)\right], \tag{D1}$$

where n denotes the oscillator Fock state, t is the duration of the sideband interaction, Ω_{SB} is the Rabi frequency of the sideband (for the $|\downarrow\rangle|n=0\rangle \leftrightarrow |\uparrow\rangle|n=1\rangle$ transition), and γ is a phenomenological decay constant. We note that Ref. [49] used a multiplier of $(n+1)^{0.7}$ for γ, while Refs. [11,55] used a multiplier of $(n+1)^{0.5}$, as is done here; this choice has a small effect on goodness of fit, but does not affect the extracted Fock state populations. The factor of $\sqrt{n+1}$ multiplying Ω_{SB} assumes that the system is in the Lamb-Dicke regime, meaning here that the microwave magnetic field gradient used to perform the sideband operation is homogeneous over the spatial extent of the ion motional wavepacket [44]. This is an excellent approximation for our system [11]. The Fock state probability distribution of the initial motional state is given by $\{P_n\}$. We fit the measured traces of $P_\downarrow(t)$ to extract the values of $\{P_n\}$. For specific classes of motional states, the $\{P_n\}$ are related in a parameterized way; for example, a coherent state parameterized by the amplitude α can be described by the model [56]

$$P_n = \frac{e^{-|\alpha|^2}|\alpha|^{2n}}{n!}, \tag{D2}$$

while the squeezed vacuum state parameterized by complex squeezing parameter $\xi = re^{i\theta}$ can be described by the model [56]

$$P_n = \frac{(\tanh r)^n}{\cosh r}\frac{n!}{2^n}\left(\frac{1}{(n/2)!}\right)^2 \tag{D3}$$

for even n, with $P_n = 0$ for odd n. Figure 6 shows example traces of the $|\downarrow\rangle$ population versus BSB duration, along with extracted motional state populations in the Fock basis. The upper plots in each panel show the extracted populations for both "model-free" fits, fitting to Eq. (D1) to determine the P_n while only constraining that $\sum_{n=0}^{\infty} P_n = 1$, as

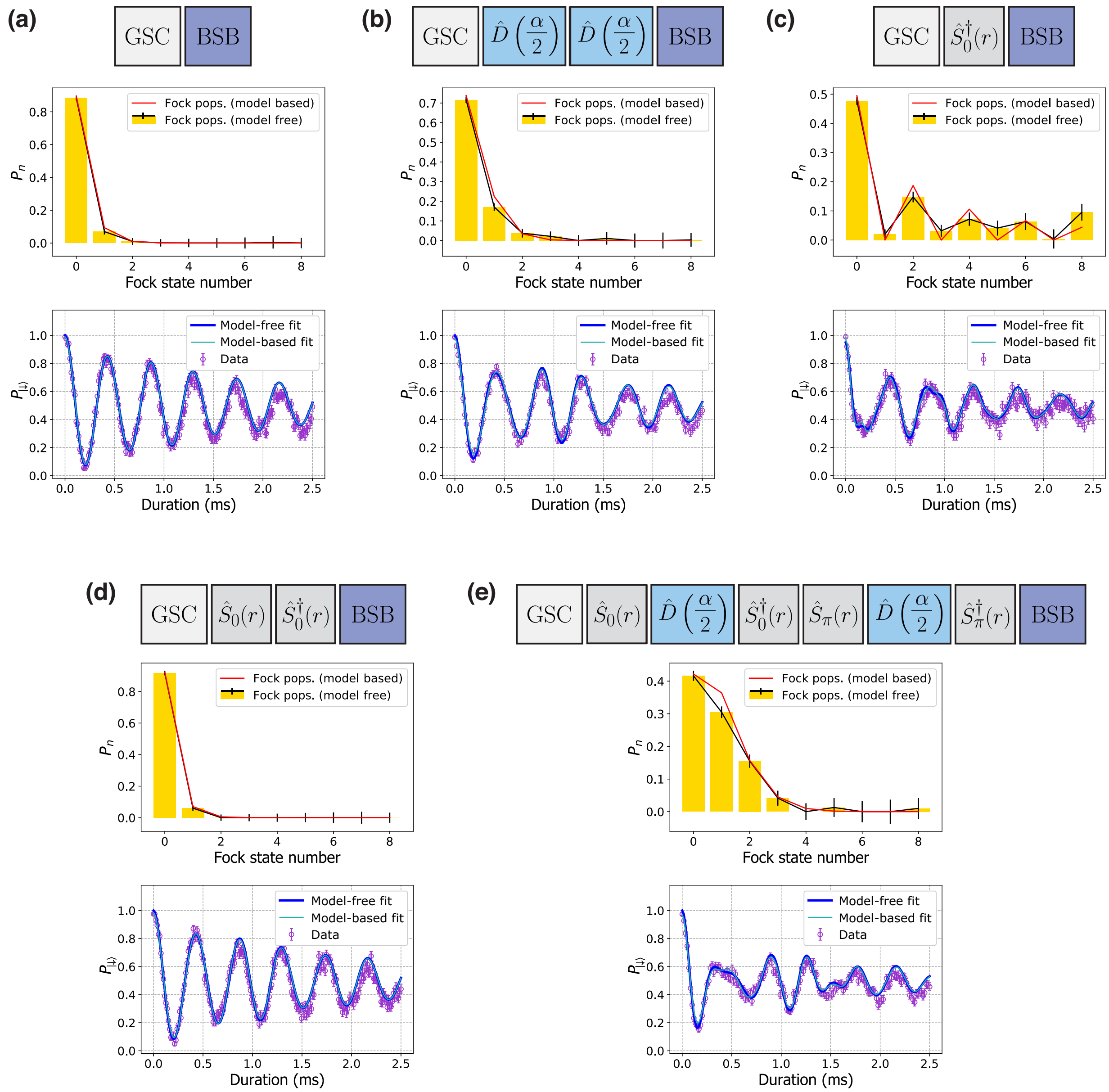

FIG. 6. Pulse sequences and calibration data for amplification of coherent displacements. GSC, ground-state cooling; BSB, blue sideband analysis pulse. Displacement and squeezing operators are the same as in Fig. 1. The lower plot in each panel shows the measured population in $|\downarrow\rangle$ (purple circles) as a function of BSB analysis pulse duration for various initial motional states. The dark blue lines show the result of model-free fits to the data from Eq. (D1), as described in the text, and the light blue lines show the model-based fits used to extract the various parameters (r, $\bar{n}$, α). Both the Fock state plots and BSB flops demonstrate good agreement between the model-based and model-free fits, validating our choice of fit models. The upper plot in each panel shows the corresponding Fock state populations extracted by fitting to the BSB oscillations. The red lines show the best-fit Fock state populations from a model-based fit to the BSB oscillations, while the yellow bars show the Fock state populations extracted from a model-free fit. The vertical black lines show 68% confidence intervals on the model-free fitted populations. Diagonal black lines connect the tops of the yellow bars to guide the eye and highlight deviations between the model-based and model-free fitted populations. (a) Ground-state cooling calibration. We find a mean occupation of $\bar{n} = 0.06(1)$. (b) Displacement calibration. Following ground-state cooling, the motional state is displaced by an applied resonant excitation pulse split into two 3.5-μs segments (7 μs total), yielding $\alpha_i = 0.55(2)$. (c) Squeezing calibration. Following ground-state cooling, the parametric drive is applied for 2.75 μs to generate a squeezed state of motion. (d) Antisqueezing calibration and squeezing coherence verification. The ion is cooled to its motional ground state, the parametric drive is applied for 2.75 μs, and then the parametric drive is applied for an additional 2.75 μs with a 180° phase shift. Fitting the resulting state to a model for a thermal state, we find that $\bar{n} = 0.09(1)$. (e) Hamiltonian amplification experiment. Final motional state after HA of a coherent displacement with $N = 1$, using two displacement pulses of 3.5-μs duration and four squeezing or antisqueezing pulses of 2.75-μs duration. The data in Fig. 3 are produced by comparing the calibrated unamplified displacement as seen in (b) to the displacement extracted in (e) for different relative phases between the displacement and squeezing pulses.

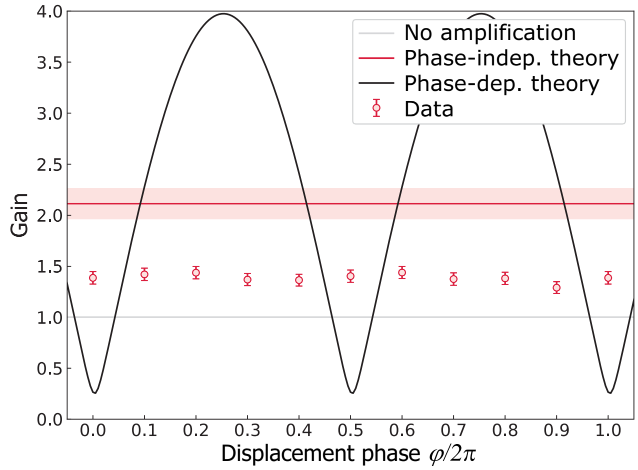

FIG. 7. HA gain versus displacement phase for $N = 3$. This plot shows the same experiment as in Fig. 3, but with $N = 3$ rather than $N = 1$. This means that the displacement is split into six equal pieces rather than two, which, due to experimental imperfections, results in decreased amplification but improved phase insensitivity. Experimental data are shown as red circles, with error bars denoting 68% confidence intervals. The red line (light red band) shows the theoretical prediction (68% confidence interval) for the HA gain $G = \cosh(r)$ given the experimentally determined value of $r = 1.38(8)$. The theoretical phase-dependent gain of the scheme in Fig. 1(a) given the same r is shown for comparison as the black line. The gray line denotes $G = 1$. The data point plotted at $\varphi/2\pi = 1$ is a copy of the data point at $\varphi/2\pi = 0$.

well as "model-based" fits, where the P_n are all related according to one of the parameterized models described above. The lower plots in each panel show the experimental data along with the corresponding model-based and model-free fit curves.

The r value reported in the main text is a mean of two squeezing calibrations, one measured before the data were taken and a second one measured after, as the actual experimental squeezing strength drifts more than is captured in the fit uncertainty. The value calibrated just before the data in Figs. 3 and 7 were taken is $r = 1.42(3)$, and the value from afterwards (just under 4 h later) is $r = 1.33(3)$. Error bars for the mean squeezing value are determined using the Student's t distribution. We suspect that these experimental drifts, along with other imperfections in the squeezing operations, are the primary factor limiting HA performance and account for a large portion of our residual phase sensitivity.

We use independent calibration experiments to fix several of the fit parameters, as well as to validate the assumptions we make when fitting. Each calibration experiment consists of preparing a desired initial state of motion, followed by a BSB analysis pulse of varying duration to extract $P_\downarrow(t)$. The first calibration experiment performs BSB analysis immediately after the ground-state cooling sequence, with no squeezing or displacement applied, as shown in Fig. 6(a). We fit the resulting trace to Eq. (D1) to determine calibrated values of γ and Ω, as well as to estimate $\bar{n}$ for the initial motional state after ground-state cooling.

Next we calibrated the squeezing and displacement operations using the fitted values for γ and Ω. The squeezing calibration consists of applying the parametric drive to squeeze the initial motional state after ground-state cooling, then performing BSB analysis to extract the value of r by fitting to a model for a squeezed ground state, as shown in Fig. 6(c). The duration of the parametric drive is the same as used to generate the squeezing operations in the HA experiments. We calibrate the displacement α by applying a series of resonant motional excitation pulses after first performing ground-state cooling, as shown in Fig. 6(b). The number and duration of displacement pulses match the values used in the HA experiments. We fit the measured BSB oscillations to a model for a coherently displaced ground state. Finally, we characterize the phase coherence of the squeezed states by performing squeezing and then antisqueezing (the latter by adjusting the phase of the parametric drive) on the ground-state-cooled motional mode and fitting the BSB oscillations to determine the amount of residual squeezing, as shown in Fig. 6(d). Based on the results of our ground state cooling, squeezing, and antisqueezing calibrations, we make the approximation for fitting purposes that the final state after an HA sequence is a coherent state of motion.

Although, for amplification of displacements, the interaction to be amplified does not need to be finely Trotterized (i.e., N does not need to be > 1) since it commutes with the squeezing operations, we performed the displacement amplification experiment with $N = 3$, the results of which are shown in Fig. 7. For $N = 3$, we split our displacement into six pieces rather than two, which triples the number of squeeze-unsqueeze pairs. This resulted in markedly better phase insensitivity, but reduced gain. Increasing the number of squeezing operations increases motional decoherence, but alternating the axes along which we amplify more frequently reduces residual phase sensitivity from imperfections in our squeeze drive.

[1] C. M. Caves, Quantum-mechanical noise in an interferometer, Phys. Rev. D **23**, 1693 (1981).
[2] B. Yurke, S. L. McCall, and J. R. Klauder, SU(2) and SU(1,1) interferometers, Phys. Rev. A **33**, 4033 (1986).
[3] M. Kitagawa and M. Ueda, Nonlinear-interferometric generation of number-phase-correlated fermion states, Phys. Rev. Lett. **67**, 1852 (1991).
[4] D. J. Wineland, J. J. Bollinger, W. M. Itano, F. L. Moore, and D. J. Heinzen, Spin squeezing and reduced quantum noise in spectroscopy, Phys. Rev. A **46**, R6797 (1992).

[5] M. Kitagawa and M. Ueda, Squeezed spin states, Phys. Rev. A **47**, 5138 (1993).

[6] L. Pezzè, A. Smerzi, M. K. Oberthaler, R. Schmied, and P. Treutlein, Quantum metrology with nonclassical states of atomic ensembles, Rev. Mod. Phys. **90**, 035005 (2018).

[7] M. Xin, W. S. Leong, Z. Chen, Y. Wang, and S.-Y. Lan, Rapid quantum squeezing by jumping the harmonic oscillator frequency, Phys. Rev. Lett. **127**, 183602 (2021).

[8] S. Colombo, E. Pedrozo-Peñafiel, A. F. Adiyatullin, Z. Li, E. Mendez, C. Shu, and V. Vuletić, Time-reversal-based quantum metrology with many-body entangled states, Nat. Phys. **18**, 925 (2022).

[9] J. Aasi *et al.*, Enhanced sensitivity of the LIGO gravitational wave detector by using squeezed states of light, Nat. Photonics **7**, 613 (2013).

[10] M. Malnou, D. A. Palken, B. M. Brubaker, L. R. Vale, G. C. Hilton, and K. W. Lehnert, Squeezed vacuum used to accelerate the search for a weak classical signal, Phys. Rev. X **9**, 021023 (2019).

[11] S. C. Burd, R. Srinivas, J. Bollinger, A. Wilson, D. Wineland, D. Leibfried, D. Slichter, and D. Allcock, Quantum amplification of mechanical oscillator motion, Science **364**, 1163 (2019).

[12] E. Davis, G. Bentsen, and M. Schleier-Smith, Approaching the Heisenberg limit without single-particle detection, Phys. Rev. Lett. **116**, 053601 (2016).

[13] O. Hosten, R. Krishnakumar, N. J. Engelsen, and M. A. Kasevich, Quantum phase magnification, Science **352**, 1552 (2016).

[14] O. Hosten, N. J. Engelsen, R. Krishnakumar, and M. A. Kasevich, Measurement noise 100 times lower than the quantum-projection limit using entangled atoms, Nature **529**, 505 (2016).

[15] I. Kruse, K. Lange, J. Peise, B. Lücke, L. Pezzè, J. Arlt, W. Ertmer, C. Lisdat, L. Santos, A. Smerzi, and C. Klempt, Improvement of an atomic clock using squeezed vacuum, Phys. Rev. Lett. **117**, 143004 (2016).

[16] K. A. Gilmore, M. Affolter, R. J. Lewis-Swan, D. Barberena, E. Jordan, A. M. Rey, and J. J. Bollinger, Quantum-enhanced sensing of displacements and electric fields with two-dimensional trapped-ion crystals, Science **373**, 673 (2021).

[17] K. M. Backes, D. A. Palken, S. A. Kenany, A. A. Droster, G. C. Hilton, S. Ghosh, and H. Jackson, A quantum enhanced search for dark matter axions., Nature **590**, 238 (2021).

[18] M. Renger, S. Pogorzalek, Q. Chen, Y. Nojiri, K. Inomata, Y. Nakamura, M. Partanen, A. Marx, R. Gross, F. Deppe, and K. G. Fedorov, Beyond the standard quantum limit for parametric amplification of broadband signals, Npj Quantum Inf. **7**, 160 (2021).

[19] M. Jiang, Y. Qin, X. Wang, Y. Wang, H. Su, X. Peng, and D. Budker, Floquet spin amplification, Phys. Rev. Lett. **128**, 233201 (2022).

[20] A. Metelmann, O. Lanes, T.-Z. Chien, A. McDonald, M. Hatridge, and A. A. Clerk, Quantum-limited amplification without instability, arXiv:2208.00024 [quant-ph] (2022).

[21] X.-Y. Lü, Y. Wu, J. R. Johansson, H. Jing, J. Zhang, and F. Nori, Squeezed optomechanics with phase-matched amplification and dissipation, Phys. Rev. Lett. **114**, 093602 (2015).

[22] M.-A. Lemonde, N. Didier, and A. A. Clerk, Enhanced nonlinear interactions in quantum optomechanics via mechanical amplification, Nat. Commun. **7**, 11338 (2016).

[23] S. Zeytinoğlu, A. İmamoğlu, and S. Huber, Engineering matter interactions using squeezed vacuum, Phys. Rev. X **7**, 021041 (2017).

[24] W. Qin, A. Miranowicz, P.-B. Li, X.-Y. Lü, J. Q. You, and F. Nori, Exponentially enhanced light-matter interaction, cooperativities, and steady-state entanglement using parametric amplification, Phys. Rev. Lett. **120**, 093601 (2018).

[25] Y.-H. Chen, W. Qin, and F. Nori, Fast and high-fidelity generation of steady-state entanglement using pulse modulation and parametric amplification, Phys. Rev. A **100**, 012339 (2019).

[26] C. Leroux, L. C. G. Govia, and A. A. Clerk, Enhancing cavity quantum electrodynamics via antisqueezing: Synthetic ultrastrong coupling, Phys. Rev. Lett. **120**, 093602 (2018).

[27] C. Arenz, D. I. Bondar, D. Burgarth, C. Cormick, and H. Rabitz, Amplification of quadratic Hamiltonians, Quantum **4**, 271 (2020).

[28] W. Ge, B. C. Sawyer, J. W. Britton, K. Jacobs, J. J. Bollinger, and M. Foss-Feig, Trapped ion quantum information processing with squeezed phonons, Phys. Rev. Lett. **122**, 030501 (2019).

[29] W. Ge, B. C. Sawyer, J. W. Britton, K. Jacobs, M. Foss-Feig, and J. J. Bollinger, Stroboscopic approach to trapped-ion quantum information processing with squeezed phonons, Phys. Rev. A **100**, 043417 (2019).

[30] P. Groszkowski, H.-K. Lau, C. Leroux, L. C. G. Govia, and A. A. Clerk, Heisenberg-limited spin squeezing via bosonic parametric driving, Phys. Rev. Lett. **125**, 203601 (2020).

[31] P.-B. Li, Y. Zhou, W.-B. Gao, and F. Nori, Enhancing spin-phonon and spin-spin interactions using linear resources in a hybrid quantum system, Phys. Rev. Lett. **125**, 153602 (2020).

[32] Q. Wang, C. Zhu, Y. Wang, B. Zhang, and Y. D. Chong, Amplification of quantum signals by the non-Hermitian skin effect, Phys. Rev. B **106**, 024301 (2022).

[33] M. Villiers, W. C. Smith, A. Petrescu, A. Borgognoni, M. Delbecq, A. Sarlette, M. Mirrahimi, P. Campagne-Ibarcq, T. Kontos, and Z. Leghtas, Dynamically enhancing qubit-photon interactions with anti-squeezing, arXiv:2212.04991 [quant-ph] (2023).

[34] W. Ge, Hamiltonian amplification: Another application of parametric amplification, Quantum Views **4**, 41 (2020).

[35] M. M. Nieto and D. R. Truax, Holstein-Primakoff/Bogoliubov transformations and the multiboson system, Fortschr. Phys. **45**, 145 (1997).

[36] H. F. Trotter, On the product of semi-groups of operators, Proc. Amer. Math. Soc. **10**, 545 (1959).

[37] M. Suzuki, Generalized Trotter's formula and systematic approximants of exponential operators and inner derivations with applications to many-body problems, Commun. Math. Phys. **51**, 183 (1976).

[38] T. Ichinose and H. Tamura, Note on the norm convergence of the unitary Trotter product formula, Lett. Math. Phys. **70**, 65 (2004).

[39] S. Seidelin, J. Chiaverini, R. Reichle, J. J. Bollinger, D. Leibfried, J. Britton, J. H. Wesenberg, R. B. Blakestad, R. J. Epstein, D. B. Hume, W. M. Itano, J. D. Jost, C. Langer, R. Ozeri, N. Shiga, and D. J. Wineland, Microfabricated surface-electrode ion trap for scalable quantum information processing, Phys. Rev. Lett. **96**, 253003 (2006).

[40] R. Srinivas, S. C. Burd, R. T. Sutherland, A. C. Wilson, D. J. Wineland, D. Leibfried, D. T. C. Allcock, and D. H. Slichter, Trapped-ion spin-motion coupling with microwaves and a near-motional oscillating magnetic field gradient, Phys. Rev. Lett. **122**, 163201 (2019).

[41] S. C. Burd, R. Srinivas, H. M. Knaack, W. Ge, A. C. Wilson, D. J. Wineland, D. Leibfried, J. J. Bollinger, D. T. C. Allcock, and D. H. Slichter, Quantum amplification of boson-mediated interactions, Nat. Phys. **17**, 898 (2021).

[42] R. Srinivas, S. C. Burd, H. M. Knaack, R. T. Sutherland, A. Kwiatkowski, S. Glancy, E. Knill, D. J. Wineland, D. Leibfried, A. C. Wilson, D. T. C. Allcock, and D. H. Slichter, High-fidelity laser-free universal control of trapped ion qubits, Nature **597**, 209 (2021).

[43] C. Monroe, D. M. Meekhof, B. E. King, S. R. Jefferts, W. M. Itano, D. J. Wineland, and P. Gould, Resolved-sideband Raman cooling of a bound atom to the 3D zero-point energy, Phys. Rev. Lett. **75**, 4011 (1995).

[44] D. J. Wineland, C. Monroe, W. M. Itano, D. Leibfried, B. E. King, and D. M. Meekhof, Experimental issues in coherent quantum-state manipulation of trapped atomic ions, J. Res. Natl. Inst. Stand. Technol. **103**, 259 (1998).

[45] D. Leibfried, R. Blatt, C. Monroe, and D. J. Wineland, Quantum dynamics of single trapped ions, Rev. Mod. Phys. **75**, 281 (2003).

[46] C. Ospelkaus, C. E. Langer, J. M. Amini, K. R. Brown, D. Leibfried, and D. J. Wineland, Trapped-ion quantum logic gates based on oscillating magnetic fields, Phys. Rev. Lett. **101**, 090502 (2008).

[47] C. Ospelkaus, U. Warring, Y. Colombe, K. R. Brown, J. M. Amini, D. Leibfried, and D. J. Wineland, Microwave quantum logic gates for trapped ions, Nature **476**, 181 (2011).

[48] D. J. Heinzen and D. J. Wineland, Quantum-limited cooling and detection of radio-frequency oscillations by laser-cooled ions, Phys. Rev. A **42**, 2977 (1990).

[49] D. M. Meekhof, C. Monroe, B. E. King, W. M. Itano, and D. J. Wineland, Generation of nonclassical motional states of a trapped atom, Phys. Rev. Lett. **76**, 1796 (1996).

[50] C. M. Caves, Reframing SU(1, 1) interferometry, Adv. Quantum Technol. **3**, 1900138 (2020).

[51] Q. A. Turchette, C. J. Myatt, B. E. King, C. A. Sackett, D. Kielpinski, W. M. Itano, C. Monroe, and D. J. Wineland, Decoherence and decay of motional quantum states of a trapped atom coupled to engineered reservoirs, Phys. Rev. A **62**, 053807 (2000).

[52] A. Rivas and S. F. Huelga, *Open Quantum Systems* (Springer, New York, New York, 2012), Vol. 10.

[53] C. Arenz, R. Hillier, M. Fraas, and D. Burgarth, Distinguishing decoherence from alternative quantum theories by dynamical decoupling, Phys. Rev. A **92**, 022102 (2015).

[54] D. A. Lidar and T. A. Brun, *Quantum Error Correction* (Cambridge University Press, Cambridge, United Kingdom, 2013).

[55] D. Kienzler, H.-Y. Lo, B. Keitch, L. de Clercq, F. Leupold, F. Lindenfelser, M. Marinelli, V. Negnevitsky, and J. P. Home, Quantum harmonic oscillator state synthesis by reservoir engineering, Science **347**, 53 (2015).

[56] C. C. Gerry and P. L. Knight, *Introductory Quantum Optics* (Cambridge University Press, Cambridge, United Kingdom, 2005).